

PWM Algorithms for Multilevel Inverter Supplied Multiphase Variable-Speed Drives

Martin Jones, Obrad Dordevic, Nandor Bodo, and Emil Levi

Abstract—Multiphase variable speed drives are nowadays regarded as serious contenders for various applications, due to the certain advantages that they possess when compared to three-phase drives. On the other hand, the multilevel (predominantly three-level) voltage source inverter (VSI) has become an industrially accepted technology for medium-voltage three-phase drives. The logical next step is to integrate multilevel VSI and multiphase drive technologies, since benefits of each can then be combined. This paper will review recent advances in this area. Two different topologies of the multiphase supply will be considered and the emphasis will be placed on appropriate pulse width modulation (PWM) techniques that can be used in conjunction with the supply structure. The first topology utilises multilevel (three-level) VSI and the machine's stator multiphase winding is star-connected with an isolated neutral point. In the second topology the winding is left open-ended and each side of the winding is connected to an isolated two-level VSI. This topology can also achieve three-level operation. Carrier-based and space vector based PWM strategies are considered and the obtainable performance is illustrated using experimental results.

Index Terms—Multiphase drives, multilevel voltage source inverters, open-end winding topology.

I. INTRODUCTION

THE requirements that a VSI modulation algorithm should satisfy are numerous. Most importantly, the output phase voltages must match the commanded references on average and the undesired harmonics should appear only around the multiples of the switching frequency. The resulting voltage total harmonic distortion (THD) should be as low as possible and the switching sequence should be arranged symmetrically, in a way that gives each inverter leg equal and constant switching frequency. The resulting voltage waveforms should have maximal dc-link utilisation. Some requirements are in contradiction to each other. For instance, switching losses can be minimised by lowering the switching frequency, however this impacts negatively on the THD and electro-magnetic interference (EMI).

Manuscript received 30 May 2012. Accepted for publication 10 June 2012. Some results of this paper were presented at the 16th International Symposium Power Electronics, Novi Sad, Serbia, October 26-28, 2012.

This paper was made possible by NPRP grant 4-152-02-053 from the Qatar National Research Fund (a member of Qatar Foundation). The statements made herein are solely the responsibility of the authors.

M. Jones, O. Dordevic, N. Bodo and E. Levi are with School of Engineering, Technology and Maritime Operations, Liverpool John Moores University, Liverpool, United Kingdom (e-mails: m.jones2@ljmu.ac.uk, o.dordevic@2009.ljmu.ac.uk, n.bodo@2009.ljmu.ac.uk, e.levi@ljmu.ac.uk).

Three-phase modulation methods are well established in terms of both carrier-based and space vector techniques. With properly chosen zero sequence that is added to the reference, the same voltage waveforms are achievable with both types of the modulation strategies [1]. The space vector techniques use the three nearest space vectors to the reference, which are the vertices of the triangle in which the reference is positioned. In the two-level case this means that two active and zero space vectors are used to achieve the reference during each switching period.

The advantages of multiphase variable speed drives over the three-phase ones are numerous [2]. An increase of fault tolerance is achieved, since the rotating field inside the stator winding can be obtained with only three phases. Thus, the machine can continue its operation with several faulted phases, as long as there are at least three healthy ones left [3]. Multiphase machines can be built with concentrated or distributed windings. With the distributed winding machines only the first harmonic of the supply contributes to torque production. However, there is a possibility to have several multiphase machines connected in series and drive them independently with a single VSI [3]-[4]. When the machine is equipped with a concentrated winding, other, higher harmonics can also be used for torque production. Therefore, a higher amount of torque is producible with a better iron utilisation than with its three-phase counterpart [2].

Three-phase multilevel topologies have been drawing increased attention in the past two decades [5]. The numerous advantages of multilevel supply include [6]: good power quality (low voltage distortion and dv/dt), good electromagnetic compatibility, operation with a lower switching frequency (lower switching losses), high voltage capability, smaller common mode (CM) voltage (reducing the stress in the motor bearings), and the possibility for fault tolerant operation in some, modular configurations. There are various topologies of multilevel converters. The main ones are the neutral point clamped (NPC), the flying capacitor (FC) and the cascaded converters [5]-[6].

Among the cascaded converters, the dual two-level inverter configuration supplying an open-end winding machine has received growing attention due to its simple structure [7]. Typically, three-phase VSIs are utilised. Application of such a dual-inverter supply enables drive operation with voltage waveform equivalent to the one obtainable with a three-level VSI in single-sided supply mode. Three-phase open-end

winding drive systems are currently considered as possible alternative supply solutions in EVs/HEVs [8]-[9], propulsion [10] and rolling mills [11].

Over the years many modulation algorithms have been presented for the three-phase multilevel converter. A general space vector based approach is given in [12] which, with some modifications, can be made applicable to any single-sided three-phase converter topology.

Although combination of a multilevel converter and a multiphase machine appears advantageous, there are relatively few examples of the multiphase multilevel drives [13]-[24]. The focus is on the three-level five-phase NPC drive [13]-[15]. The initial space vector modulation (SVM) methods for multiphase VSIs were based on the simple extension of the three-phase multilevel SVM approaches, so that only the three vectors were utilised. Such an extension from the three-phase to five-phase system, that divides each sector into four equal triangles, is given for three-level inverter in [14]. An optimal SVM switching strategy, based on a discrete particle swarm optimisation (PSO) algorithm, is presented in [13]. In principle, the number of applied vectors must equal the number of phases [3]. Utilisation of three instead of five space vectors during the switching period disregards this basic rule; consequently, only the first plane of the multiphase system is controlled. Hence numerous low-order harmonics are generated, which map into the second plane. Another similar concept, again based on the three-phase principles, is also used in [14].

A SVM method, which controls both planes, has been developed in [15] for the three-level NPC five-phase drive and is extended to the seven-phase case in [16]. Further details of this SVM technique will be presented later on in the paper. A different approach to the SVM of multilevel multiphase system is given for a general case of an m -level, n -phase VSI in [17]. The algorithm is based on the considerations of the multidimensional (n -dimensional) space and therefore does not include decomposition of the n -dimensional space into 2-D planes. A somewhat similar method, in the sense that decomposition into 2-D planes is not utilised, is the one in [18], where a multiphase multilevel PWM is developed using n single-leg modulators.

Initial interest in the multiphase drive systems in open-end winding configuration was limited to an asymmetrical six-phase induction motor drive. In [19] the supply is provided by means of two isolated two-level six-phase VSIs. The goal was, in essence, low-order harmonic reduction rather than the multilevel operation. As a consequence, the converter is not operated in multilevel mode. The scheme considered in [20] employs four three-phase two-level inverters, with four isolated dc sources to prevent circulation of zero sequence currents. The SVM control is performed in the same way as for a standard three-level three-phase converter, using the nearest three vector (NTV) approach in conjunction with three-level NPC inverter. The work is focused towards controlling the power sharing between the four converters. Recently, modulation techniques have been proposed for the five-phase [21]-[23], seven-phase and nine-phase [24] open-end winding topologies. These modulation algorithms will be

discussed in detail in this paper and their performance examined using two experimental set-ups.

II. TWO-LEVEL MULTIPHASE SPACE VECTOR MODULATION

Before considering multilevel multiphase modulation techniques it is beneficial to review the two-level SVM method [25]. This method serves as a benchmark for other modulation methods and it comprises the basic ideas that are used further in the development of other modulation techniques. Similarly to the three-phase inverters, the ones with more phases also consider space vectors to calculate the switching states and their application times.

Common for all n -phase (where n is an odd number) sinusoidal SVM schemes is the need to use $n-1$ active space vectors per switching period. Once when the set of $n-1$ active space vectors is identified and the reference space vector magnitude and position are known, it is necessary to solve an algebraic set of $n-1$ equations, in order to obtain duty cycles of each active space vector. These equations are generated considering positions and magnitudes of the selected active space vectors in all of the $(n-1)/2$ 2-D planes. The aim is to generate the fundamental in the first plane, while zero average value is imposed as the restriction in all the other planes.

Fig. 1 shows the two-level VSI five-phase space vector pattern, which is the same in both of the planes of the topology. Space vectors are labeled with decimal numbers, which, when converted into binary, reveal the values of the switching functions of each of the inverter legs. Active (non-zero) space vectors belong to three groups in accordance with their magnitudes - small, medium and large space vector groups. The magnitudes are identified with indices s , m , and l and are given as $|\underline{v}_s| = 4/5\cos(2\pi/5)V_{dc}$, $|\underline{v}_m| = 2/5V_{dc}$, and $|\underline{v}_l| = 4/5\cos(\pi/5)V_{dc}$, respectively. The switching states that produce large vectors in the α - β plane map into small vectors in the x_1 - y_2 plane and vice-versa. The space vectors clearly divide the plane in ten sectors, each occupying a 36° angle around the origin. The next step in the multiphase SVM is to choose the space vectors to be applied. The aim is to apply the space vectors with the largest magnitudes in the first plane, and the smallest magnitudes in the other plane(s) [25]. The solution for five-phase case is depicted in Fig. 2 with the mapping of the space vectors in the first and the second plane. The projections of the reference signal to the axis of the applied space vectors in both planes enable the derivation of their dwell times according to:

$$t_{bl} = \frac{2 \sin(2\pi/5)}{V_{dc}} \sin[\vartheta - (s-1)\pi/5] |\underline{v}^*| t_s \quad (1)$$

$$t_{bm} = \frac{2 \sin(\pi/5)}{V_{dc}} \sin[\vartheta - (s-1)\pi/5] |\underline{v}^*| t_s$$

$$t_{al} = \frac{2 \sin(2\pi/5)}{V_{dc}} \sin(s\pi/5 - \vartheta) |\underline{v}^*| t_s \quad (2)$$

$$t_{am} = \frac{2 \sin(\pi/5)}{V_{dc}} \sin(s\pi/5 - \vartheta) |\underline{v}^*| t_s$$

where t_s is the switching period, ϑ is the reference position and indices a and b are defined in Fig. 2. Total time of application

of the zero space vector $t_0 = t_s - (t_{a1} + t_{am} + t_{bl} + t_{bm})$ is equally shared between zero space vectors \underline{v}_0 and \underline{v}_{31} . The vectors are then arranged in a switching sequence that is symmetrical and gives equal switching frequency in each inverter leg.

As an example of the performance of this method, an experimental result is presented in Fig. 3. The switching frequency is 2kHz, the modulation index is $M = 1$ and the dc-link voltage is 600V. Inverter dead time is 6 μ s and the load is a five-phase R-L type. Clearly the algorithm generates practically no low order harmonics with the dominant harmonics positioned around multiples of the switching frequency. Furthermore, the target fundamental frequency (50Hz) and amplitude are met.

III. MULTIPHASE MULTILEVEL TOPOLOGIES

Multiphase machines can be built using two different concepts for the torque production. In the one considered throughout this paper, the winding is wound in such a way that the magneto-motive force distribution can be regarded as near-sinusoidal. As a consequence, the supply is required to provide only fundamental harmonic, without any low-order harmonics in the motor voltage waveform. Thus, the reference phase voltages are sinusoidal.

In the first considered topology three-level NPC VSI is used to supply the machine with, in principle, n -phase stator winding and single isolated neutral point. The topology is

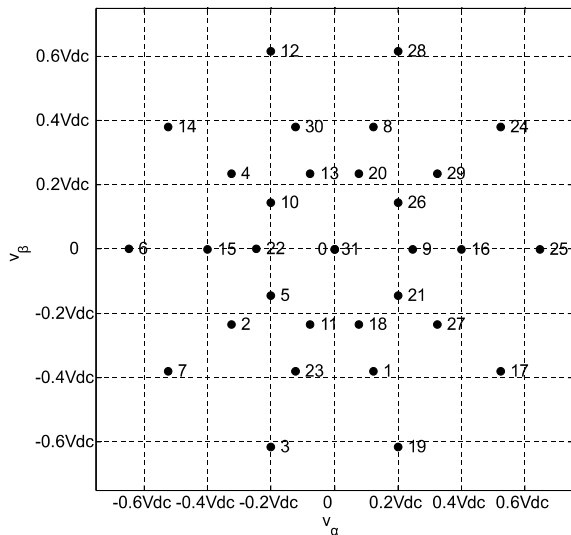


Fig. 1. Two-level five-phase VSI space vector pattern.

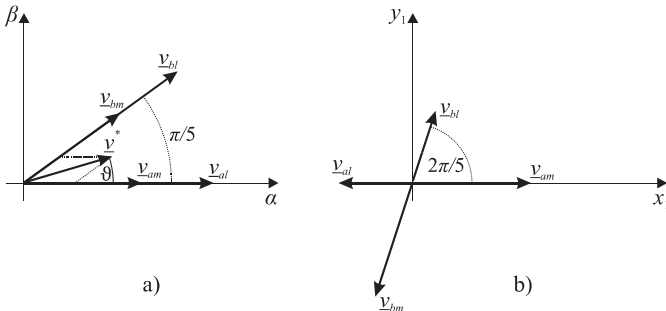


Fig. 2. Reference and applied space vectors in the first sector of the five-phase two-level VSI supply in (a) the first and (b) the second plane.

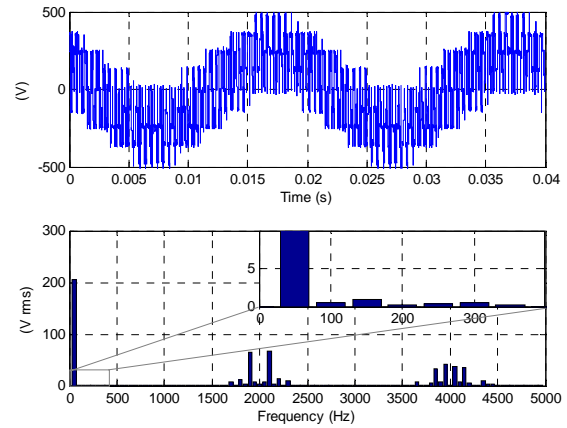


Fig. 3. Experimental result: phase voltage for five-phase two-level SVM with R-L load ($M = 1$).

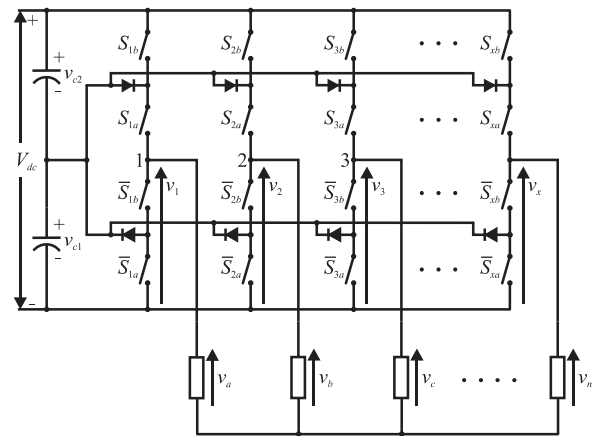


Fig.4. Multiphase (n -phase) three-level NPC inverter supplying a star connected load.

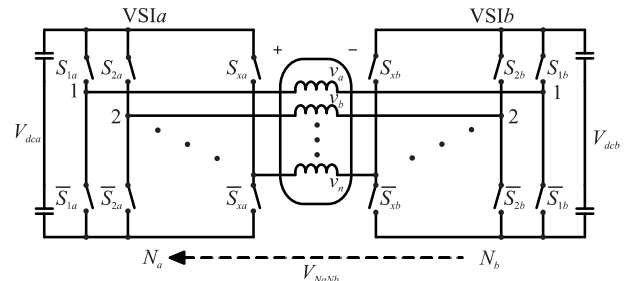


Fig. 5. Open-end winding supply structure.

shown in Fig. 4. This paper considers predominantly five-phase (and, to some extent seven-phase) topology, although the same principles of PWM control can be extended to symmetrical multiphase machines with a composite phase number and machines with an asymmetrical multiphase winding (e.g., two three-phase windings mutually shifted by 30 degrees).

The second discussed topology, with an open-end winding structure and dual-inverter supply, is shown in Fig. 5. Two dc sources are isolated, so that the circulating current does not appear. When the dc sources are of the same voltage, as it is assumed throughout this paper, the supply configuration of Fig. 5 becomes analogous to the three-level inverter supply of Fig. 4 with doubled input dc-link voltage.

The control of multiphase multilevel converters increases in complexity with the increase of phase and level numbers of the topology. To emphasise the complexity of the problem, an illustration of the relationships between numbers of levels m and phases n , in conjunction with the number of inverter switching states and voltage space vectors, is given in Table I for the NPC VSI topology. It can be seen from Table I that an increase in the number of phases dramatically increases the number of switching states, the number of space vectors and the number of redundant switching states (the difference between the total numbers of switching states and space vectors).

Table II shows the number of space vectors and switching states for the open-end topology for odd phase numbers. It is considered, for the sake of simplicity, that the open-end topology comprises two inverters with m levels each. The increase in the space vector and switching state number is far more evident in the open-end topology, for the given phase number and the number of levels, when compared to the single-sided supply (Table I). Simultaneous increase of both leads to practically exponential rise in the number of switching states and voltage space vectors.

Comparison of Table I and Table II shows that the number of switching states in the open-end winding topology, when two-level inverters are applied at both sides, coincides with the number of switching states of the four-level single-sided inverter. On the other hand, the number of space vectors equals the number obtained with the three-level inverter. This can be explained using Table III (discussed later), which shows that, although there are four possible switching states to apply, the two-level open-end supply gives inverter states equivalent to the three-level inverter. The same can be observed in conjunction with the three-level open-end topology and the nine- and five-level single-sided inverters.

Distribution of the phase voltage space vectors in the α - β plane is depicted in Figs. 6 and 7 for the five-phase and seven-phase three-level topologies, respectively. It is evident that designing a suitable modulation method represents a significant challenge.

IV. SINGLE-SIDED MULTILEVEL MULTIPHASE MODULATION TECHNIQUES

In what follows the modulation techniques, suitable for multiphase three-level converters, will be discussed and their performances analysed using an experimental set-up illustrated in Fig. 8. The level-shifted phase-disposition PWM (PD-PWM) method will be reviewed since it has been proven to produce the best results in terms of voltage THD. A space vector modulation, introduced in [15], will be discussed next.

A. Carrier-Based Modulation

Fig. 9 shows three carrier-based PWM techniques, as utilised in the single-sided supply mode in conjunction with three-level VSIs. The phase-shifted PWM (PS-PWM) and the level-shifted PWM (LS-PWM) have appeared as a natural extension of the traditional carrier-based PWM for two-level inverters. The PS-PWM is well suited for the FC multilevel

TABLE I
NUMBER OF SWITCHING STATES AND VOLTAGE SPACE VECTORS (IN BRACKETS) IN SINGLE-SIDED CONFIGURATION

m/n	3	5	7	9
2	8 (7)	32 (31)	128 (127)	512 (511)
3	27 (19)	243 (211)	2,187 (2,059)	19,683 (19,171)
4	64 (37)	1024 (781)	16384 (14,197)	262,144 (242,461)
5	125 (61)	3,125 (2,101)	78,125 (61,741)	1,953,125 (1,690,981)
9	729 (217)	59,049 (26,281)	4,782,969 (2,685,817)	$\sim 3.9e+8$ ($\sim 2.5e+8$)

TABLE II
NUMBER OF SWITCHING STATES AND VOLTAGE SPACE VECTORS (IN BRACKETS) IN OPEN-END WINDING CONFIGURATION

m/n	3	5	7	9
2	64 (19)	1024 (211)	16,384 (2059)	262,144 (19,171)
3	729 (61)	59,049 (2101)	4,782,969 (61,741)	$\sim 3.9e+8$ (1,690,981)
4	4096 (127)	1,048,576 (9031)	$\sim 2.7e+8$ (543,607)	$\sim 6.9e+10$ ($\sim 3.0e+7$)
5	15,625 (217)	9,765,625 (26,281)	$\sim 6.1e+9$ (2,685,817)	$\sim 3.8e+12$ ($\sim 2.5e+8$)

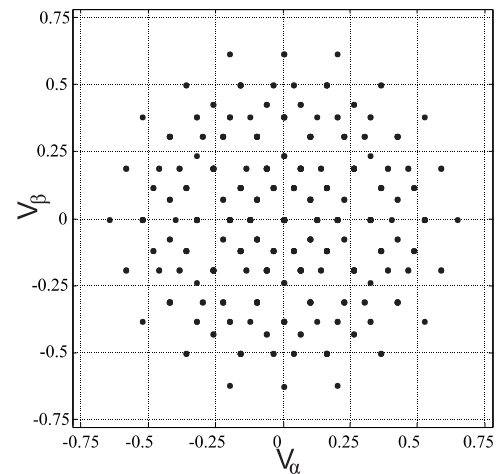


Fig. 6. Five-phase three-level VSI space vector distribution in the α - β plane.

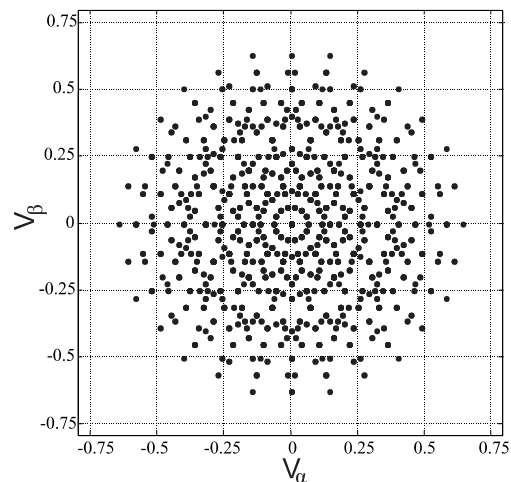


Fig. 7. Seven-phase three-level VSI space vector distribution in the α - β plane.

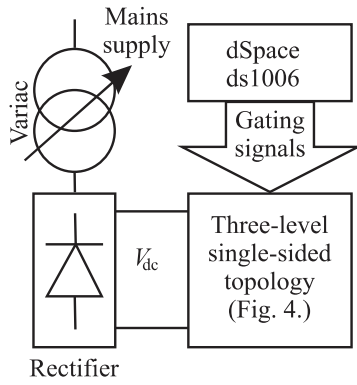


Fig. 8. Single-sided three-level VSI experimental set-up.

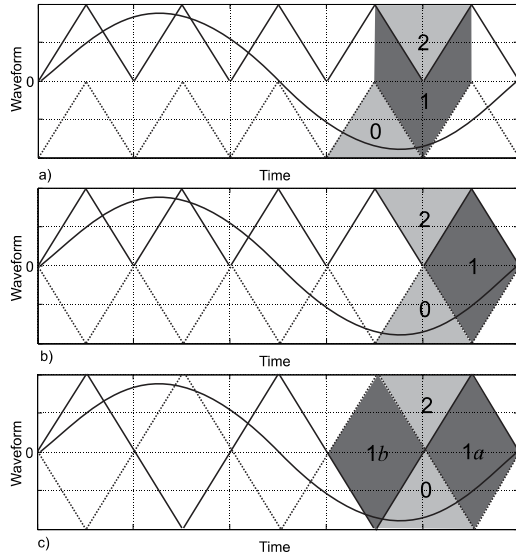


Fig. 9. Carrier and modulating signals for: a) PD-PWM, b) APOD-PWM and c) PS-PWM modulation methods.

topology because of its natural capacitor voltage balancing property. In the PS-PWM a phase shift is introduced between the carrier signals of the cells belonging to the same inverter leg, causing them to switch at different instants. A stepped multilevel waveform is created in this way [26]. The three-level structure consists of two such cells. The lowest THD is achieved when the carriers are in anti-phase. Since all the cells are effectively controlled with the same carrier that is altered only in terms of phase, i.e. the carriers occupy the same vertical position (Fig. 9c), the switch utilisation and the average power handled are evenly distributed among the cells at all times [26]. When applied to the FC topology, the capacitors are charged at the start-up. Because of the even power distribution, there will be no further unbalance produced [27]. With a topology with k cells, the output phase voltage has a switching pattern with k times the frequency of the pattern of each cell. Thus, the first higher frequency harmonics will appear at the frequencies around k (here the value is $k = 2$) times the carrier frequency [26].

Level-shifted PWM is also a natural extension of bipolar PWM. The use of a carrier signal comparison with the reference decides between the upper and lower voltage levels, which are the positive and negative dc-link rails in the case of

a two-level VSI. For a multilevel inverter, there are $(m-1)$ carriers, where m is the number of voltage levels. They are now vertically shifted rather than phase-shifted (Figs. 9a and 9b). Since each carrier determines a border between two voltage levels, the notion of ‘level-shifted’ is used. The control signals have to be sent to the appropriate switches in order to generate gating signals that correspond to the desired voltage levels and this depends on the actual inverter topology that is used.

There are several forms of the LS-PWM method. When all carriers are in phase with each other, the method is called phase disposition (PD-PWM, Fig. 9a). when all the positive carriers are in phase with each other and in phase opposition with the negative carriers, the method is known as phase opposition disposition (POD-PWM). Finally, the alternate phase opposition disposition method (APOD-PWM) is obtained by having opposite phase for each two adjacent carriers [28]. In the three-level case, POD-PWM and APOD-PWM are identical, Fig. 9b. Because of the very good characteristics and its dominance in industrial applications, PD-PWM is the method that is normally denoted as the LS-PWM in literature. LS-PWM leads to less distorted voltages, compared to PS-PWM. However, PD-PWM cannot achieve capacitor voltage balancing in the FC inverters and therefore it has to be applied to NPC inverters.

Experimental results for described five-phase PD-PWM three-level algorithm (with offset injection) are shown in Fig. 10. The data are: modulation index $M = 1$, fundamental frequency $f = 50\text{Hz}$, dc-link voltage $V_{dc} = 600\text{V}$, switching frequency $f_s = 2\text{kHz}$, and inverter dead-time $6\mu\text{s}$. Comparison with Fig. 3 shows that multilevel operation is obtained. The zero space vector is not applied in each switching period, which enables closer approximation of the reference by the applied space vectors. The number of phase voltage levels is difficult to determine from the figure but is verified as 15.

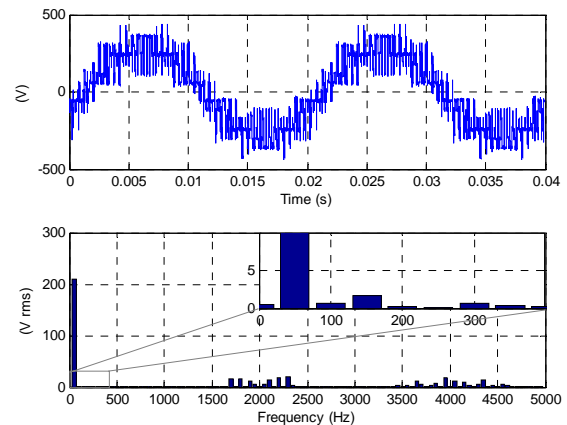


Fig. 10. Experimental result: PD-PWM carrier-based five-phase three-level case with $R-L$ load ($M = 1$).

B. Space Vector Approach

This sub-section reviews the only known SVM algorithm suitable for five-phase single-sided three-level NPC drives [15], which considers simultaneously both planes. Extension

of this algorithm to seven-phase three-level system is given in [16]. The algorithm requires a significant number of offline calculations that makes generalisation difficult. However, the final modulator structure is quite easy to implement.

The main concepts of the algorithm are briefly reviewed here. As with all space vector methods the starting point is vector space decomposition (VSD). Sinusoidal output is desired so that the reference projection into the α - β plane is circular, while projection into other planes is zero. Number of space vector projections in each plane is large (see Table I) but some of them can be omitted from further analysis. One simple rule for reduction of the number of switching states of interest is introduced in [15] and is termed the order-per-sector law [16]. Namely, the order of leg voltages must be the same as the order of the reference phase voltages in every instant of time. The order of the reference phase voltages is constant for each sector. For example, in five-phase case, order of the reference phase voltages in the first sector is $v_a^* \geq v_b^* \geq v_e^* \geq v_c^* \geq v_d^*$. The projection of the switching state 22011 belongs to the first sector in the α - β plane but it does not follow the reference order since output leg voltage v_3 is lower than v_4 ($0 < 1$). Thus, according to the order-per-sector law, this switching state can be omitted from the further analysis. The number of switching states of interest in five-phase three-level case is reduced in this way from 243 to 113, while reduction in seven-phase three-level case is from 2187 to 297.

For determination of the switching sequences one method with graphical interpretation is introduced in [16]. The one-level transition in the I^{th} leg maps into a $2/n$ scaled unit vector inclined for $(I-1) \cdot 2\pi/n$ radians with respect to α -axis. For instance, all transitions in the first sector between space vector projections after the order-per-sector law application, for five-phase three-level case, are shown in Fig. 11. Transitions in different legs are shown in different colours. Since during the switching period a transition appears in each leg, it is enough to find all closed n -angle contours (patterns) that contain each colour shown in Fig. 11. One such n -angle contour is highlighted in Fig. 11. The process of switching sequence determination is not finished at this stage, since sequence of the highlighted five transitions can start from three different switching states (10000, 11000 and 11001). In five-phase three-level case the number of patterns is 16 and there are 32 corresponding redundant switching sequences. In seven-phase three-level case these values are 64 and 128, respectively.

The space vector dwell times are calculated by solving a matrix similar to equations (1) and (2). Application of the simple rule [15], that dwell time of each switching state must be in the range from 0 to t_s , enables identification of region where the switching pattern can be applied. In other words, a number of sub-sectors are determined within each sector. In the five-phase case only 10 patterns are considered since the other six patterns have projections in x_1 - y_1 plane that cannot be cancelled in a manner similar to that shown in Fig. 2b. In seven-phase case one more non-flux/torque producing plane is present, so the situation is more difficult. There are patterns

that provide cancellation in one plane only, and patterns that provide cancellation in both planes but the dwell-time solution does not coincide. Therefore, the method of graphical elimination of some patterns is not enough, and the dwell time determination matrix has to be solved. For that purpose numerical calculations were used in [16]. After elimination of the unusable patterns, one gets that in seven-phase three-level case there are 18 patterns that divide the first sector into 18 sub-sectors. In both the five- and seven-phase case, final switching sequence per pattern is chosen by optimisation, which is simply based on the minimisation of the transitions when the reference changes sub-sector. It is preferable that all switching sequences have the same starting switching state, if it is possible. Another rule for final sequence determination is related to the inverter topology. For the best capacitor voltage balancing, those switching sequences with the maximum number of 'ones' (state when the output is determined by the mid-point of the inverter) are desirable.

To determine the sub-sector in which the reference lies, it is enough to calculate the projection of the reference to a few specified axes. These axes are determined by the borders between sub-sectors. In both five-phase and seven-phase three-level cases there are five different directions of the borders, so five projection axes are used in both cases. Comparing projections of the reference to these axes with the projection of the sub-sector borders, simple rules for sub-sector determination can be obtained.

Despite the complicated nature of the algorithm the final modulator realisation is quite straightforward, with many of the calculations performed off-line. For each sub-sector switching sequence is stored in memory. Also, dwell times calculation that requires inversion of the matrices can be calculated in advance for each switching sequence and stored in memory.

Experimental results for described five-phase three-level SVM algorithm are shown in Fig. 12. The data are: modulation index value $M = 1$, fundamental frequency $f = 50\text{Hz}$, dc-link voltage $V_{dc} = 600\text{V}$, and switching frequency $f_s = 2\text{kHz}$. Dead-time of the inverter is $6\mu\text{s}$.

The strong resemblance of the phase voltage waveform, obtained using the described SVM and carrier-based PD-

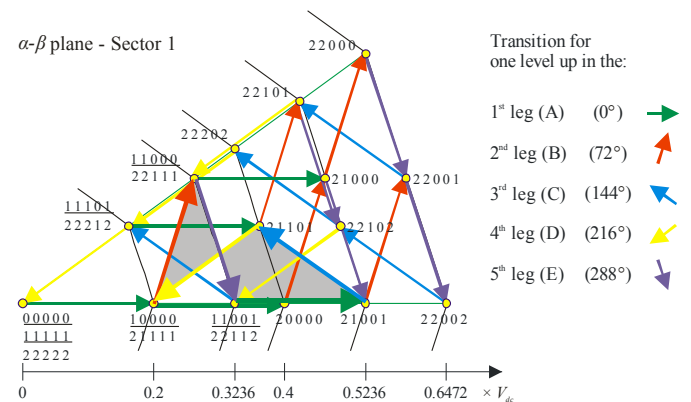


Fig. 11: All switching state transitions in the first sector after application of order-per-sector law ($n = 5$, $m = 3$).

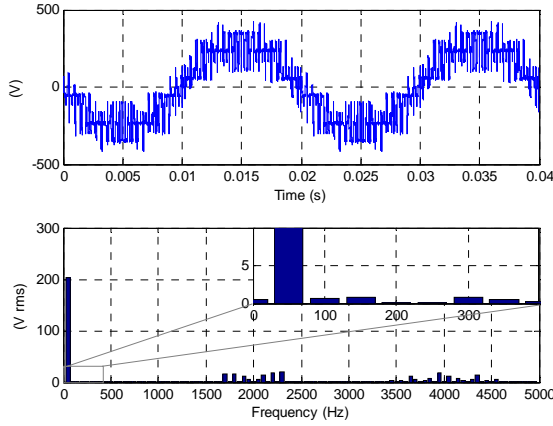


Fig. 12. Experimental result: five-phase three-level SVM with R - L load ($M=1$).

PWM methods, is evident from Figs. 10 and 12. An additional comparison, related to the phase voltage THD, is given in section 6. However, differences between the algorithms are present in the leg voltages and the CM voltage.

V. OPEN-END WINDING MULTILEVEL MULTIPHASE MODULATION TECHNIQUES

A different approach to achieve a multilevel supply is to connect two separate inverters to the ends of the stator windings, as shown in Fig. 5. There are additional benefits gained from this topology, compared to the multilevel multiphase ones. An additional degree of fault tolerance is available since the supply is realised with two independent inverters. In case one of them is faulted, the other can continue to provide power to the machine [29]. The same phase voltages can be achieved with half the dc-link voltages on the two inverter inputs compared to the single-sided supply, which can be useful in applications such as electric and hybrid electric vehicles and medium sized ships, where the dc voltage levels are limited. These applications are able to generate isolated power supplies from two sets of batteries or generators. Further, due to the construction of the topology, it can be noticed that the structure does not require additional diodes and capacitors like the NPC and FC topologies. The latter results in a further advantage: the absence of need for capacitor balancing techniques.

The easiest way to understand how the open-end topology achieves three-level operation is to compare the switching states to those of the FC converter as described in Table III. The notation for the switches for the FC topology is such that states of the upper-most and the second upper-most switch are identified with indices a and b , respectively. The notation of the switches of the open-end topology corresponds to Fig. 5, with indices a and b denoting the left and the right inverter. It can be seen that the difference between the two sets of gating signals is that those for the switches S_{xb} (x = leg number) are inverted in the open-end topology, compared to the FC. As a consequence of the topology, the load voltages are governed by the difference of voltages applied by the two inverters. In what follows three different modulation approaches will be

TABLE III
INVERTER STATES AND RELATED GATING SIGNALS

Switching function	FC VSI gating signals	Dual-inverter gating signals
2	$S_{xa}=1, S_{xb}=1$	$S_{xa}=1, S_{xb}=0$
1	1a $S_{xa}=1, S_{xb}=0$	$S_{xa}=1, S_{xb}=1$
	1b $S_{xa}=0, S_{xb}=1$	$S_{xa}=0, S_{xb}=0$
0	$S_{xa}=0, S_{xb}=0$	$S_{xa}=0, S_{xb}=1$

examined using the five-phase experimental set-up shown in Fig. A1. The equivalent total dc-link voltage is 600V, meaning 300V per inverter.

A. Space Vector Approach – URS Modulation

Due to the large number of switching states and space vectors generated by the open-end winding topology, it is prudent to try to reduce the complexity of the problem by considering the modulation in terms of two independent two-level modulators. Therefore, the two-level space vector modulation, described in section 2, can be applied to the two inverters separately.

To accommodate the fact that the inverters are located at opposite sides of the stator windings, the references applied to them are in counter-phase. This method is termed unequal reference sharing (URS) modulation since the voltage reference applied to the modulators is apportioned according to the modulation index M [21]. Initially, only $VSIa$ is operated up to its maximum modulation index ($M_1 = M_{\max} = 1.0515$ for five-phase topology), while $VSIb$ is kept in zero state. Hence the converter operates in two-level mode, since $VSIb$ output is zero (it is kept in a zero state at all times). When $M > M_{\max}/2$, $VSIa$ is held at $M_1 = M_{\max}$ and $VSIb$ output is modulated as well. The constraints of the modulation index sharing can be expressed as:

$$0 \leq M \leq M_{\max} / 2 \quad \begin{cases} M_1 = 2M \\ M_2 = 0 \end{cases} \quad (3)$$

$$M_{\max} / 2 \leq M \leq M_{\max} \quad \begin{cases} M_1 = M_{\max} \\ M_2 = 2M - M_{\max} \end{cases}$$

At lower modulation indices the second inverter is clamped to a zero vector, while the first inverter works in classical two-level modulation. Since it switches half the dc-link voltage of an equivalent single-sided two-level inverter, it is expected to give superior THD performance. In the upper modulation region the open-end topology works in multilevel mode and thus it gives better performance than the single two-level inverter.

An example of the obtained experimental results is presented in Fig. 13 where $M = 1$ and switching frequency is 1kHz. It is clear that, despite the low switching frequency, there are no low order harmonics and the target fundamental has been met.

B. SVM Approach – Decomposition Method

The complexity of selecting the proper switching states for a given command voltage can be significantly reduced if the three-level space vector decagon is decomposed into a number

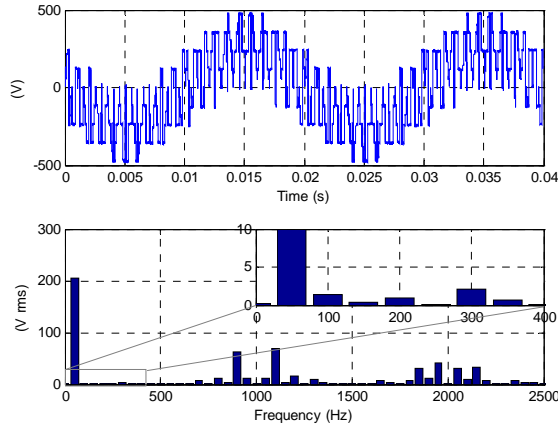


Fig. 13. Experimental result: five-phase SVM, URS method with pure R load ($M = 1$).

of two-level decagons, as illustrated in Fig. 14. The centre decagon comprises vectors which can be activated if one inverter is used up to half of the achievable maximum voltage with the other one in zero state. As a consequence, the converter is in two-level mode of operation based on four active and zero vector application, as discussed in section 2. The origins of the outer decagons are located on the outer vectors of the inner decagon, denoted by the larger dots in Fig. 14, which correspond to the outermost vectors and switching states given in Fig. 1. However, once when the magnitude of the reference voltage exceeds the maximum value obtainable with one inverter, one inverter is operated in ten-step mode while the second inverter is space vector modulated [22].

It is well known that operation of a five-phase inverter in ten-step mode without a controllable dc-link leads to uncontrollable, constant fundamental output voltage magnitude and unwanted low order harmonics. This leads to the requirement that the second inverter must be able to not only control the fundamental but also eliminate the unwanted low order harmonics, which are produced by applying only the large vector in α - β plane from the first inverter. This causes unwanted harmonics in both planes since a large vector has a corresponding non-zero value in the second, x_1 - y_1 plane. In order to achieve this objective, the second inverter modulation scheme will need to operate in both the α - β and the x_1 - y_1 planes, since references for the second inverter can be given as:

$$\begin{aligned} \underline{v}_{\alpha}^{**} &= -(\underline{v}_{\alpha}^* - \underline{v}_{i(\alpha)}) & \underline{v}_{\beta}^{**} &= -(\underline{v}_{\beta}^* - \underline{v}_{i(\beta)}) \\ \underline{v}_x^{**} &= \underline{v}_{i(x_1)} & \underline{v}_y^{**} &= \underline{v}_{i(y_1)} \end{aligned} \quad (4)$$

Here $i = 1 \dots 10$ stands for the large vector of the first VSI. A space vector modulator, which achieves simultaneous control in both the α - β and x_1 - y_1 planes, was developed in [30] in order to control multiphase multi-motor drive systems. A schematic illustration of the SVM process is shown in Fig. 15. This SVM method utilises two two-level five-phase space vector modulators, as discussed previously. Each SVM operates in a separate plane.

Fig. 16 shows the performance of the method when $M = 1$ and $f_s = 2\text{kHz}$. It is clear that a multilevel output is achieved

and that the scheme is able to completely compensate unwanted low order harmonics created by the ten-step operation of one inverter.

C. Carrier-Based Approach – PD-PWM

The carrier-based methods described in sub-section 4.1 are all applicable to the open-end winding topology. The gating signals for the two inverters are easily obtainable by associating each of the carrier signals to one inverter. Due to the differences in the inverter switching functions and their

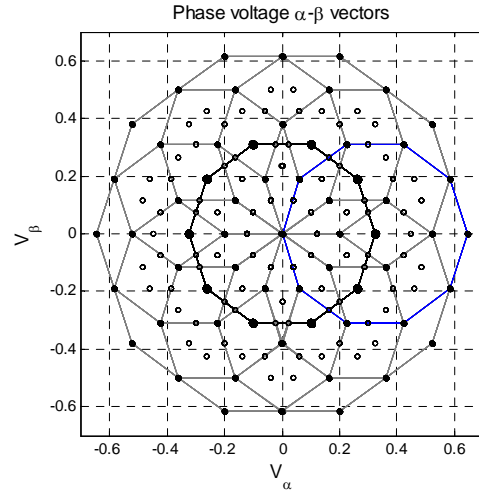


Fig. 14. Decomposed SVM method: space vector distribution in the α - β plane.

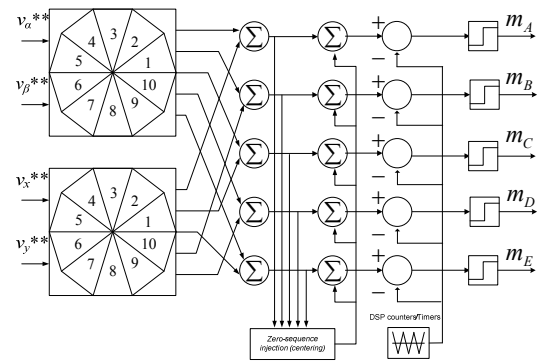


Fig. 15. Signal flow of the five-phase multi-frequency space vector modulator.

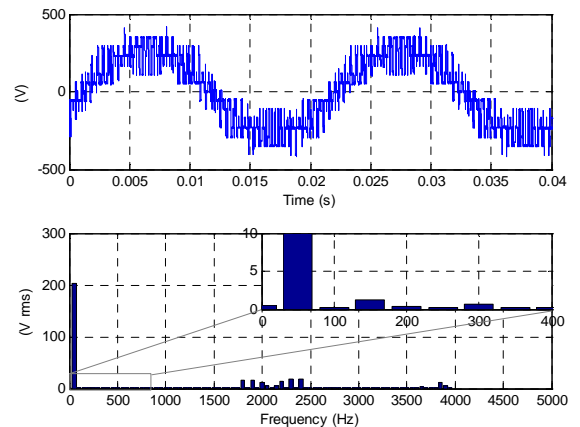


Fig. 16. Experimental result: five-phase SVM, decomposition method with R - L load ($M = 1$).

associated gating signals (Table III), one of the gating signals has to be inverted. As it was already stated, the PD-PWM gives the best results in terms of voltage THD, but it cannot be applied to the FC topology due to capacitor balancing issues. However, since there are no capacitor voltages to balance in the open-end topology, there is no restriction towards the implementation of this method.

The experimental results in Fig. 17 are obtained by applying the carrier-based PD-PWM method to the open-end winding machine. The two isolated dc-bus voltages are set to 300V. The modulation index is set to $M = 1$ and switching frequency is 2kHz. The resulting phase-voltage waveform and its harmonic spectrum are similar to the ones obtained in the previous section with the single-sided three-level inverter. These results validate the theoretical consideration that the open-end topology can work as a three-level inverter although it comprises two, more common, two-level inverters.

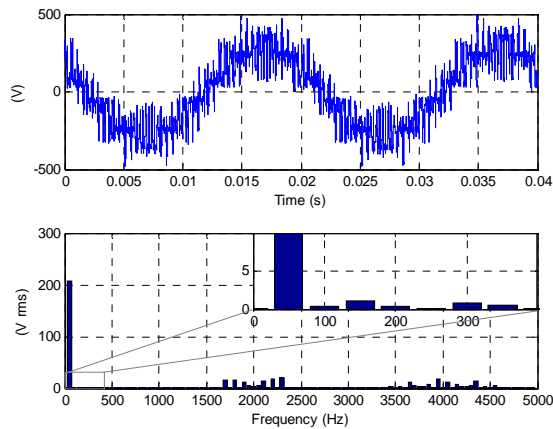


Fig. 17. Experimental result: five-phase PD-PWM method with R - L load ($M = 1$).

VI. COMPARISON OF SIMULATION AND EXPERIMENTAL RESULTS

Experimental results have been used throughout this paper to support the theory. Extensive simulation studies have, however, been also conducted and there is a very good agreement between the results obtained experimentally and via simulation. Therefore the simulation results of Fig. 18 enable a THD performance comparison between the modulation methods, investigated in the paper. As expected, the two-level VSI modulation has shown the worst performance of all the methods considered. The three-level PD-PWM and the method introduced in [15] have identical voltage THD throughout the modulation index range (the difference between them can be noticed only in the leg and CM-voltage waveforms). The URS method, developed for the open-end winding machines, has the superior performance in the low modulation region, which is the same as with the PD-PWM. However, in the upper modulation region it gradually approaches the performance of the two-level modulation. This drawback is however counter-balanced by the power-sharing capability of this method, which is important in certain applications.

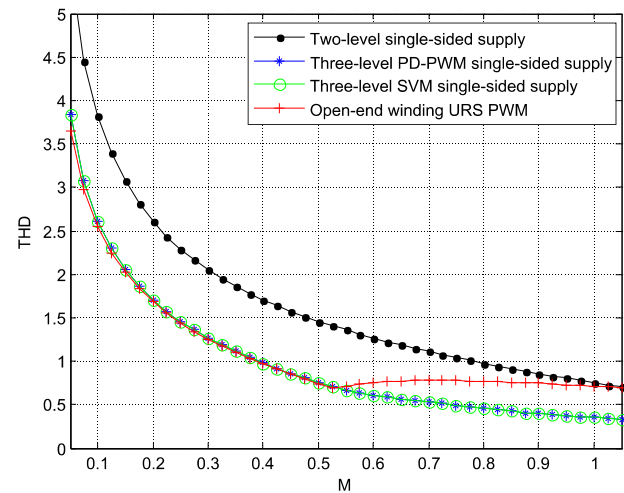


Fig. 18. Voltage THD comparison across the modulation range for a five-phase system.

VII. CONCLUSION

The combined advantages offered, by multiphase and multilevel topologies, make them an attractive proposition for high power and fault tolerant applications. However, the control of these topologies represents a considerable challenge due to the exponential increase in the number of switching states and large number of active space vectors. This paper has presented a review of some of the recently published solutions to the modulation of multiphase multilevel converters for both carrier-based modulation and SVM methods. The performance of these techniques has been examined using experimental rigs, with the THD comparison obtained by means of simulations.

REFERENCES

- [1] D. G. Holmes, "The general relationship between regular-sampled pulse-width-modulation and space vector modulation for hard switched converters," in *Proc. IEEE Industry Applications Society Annual Meeting IAS*, Houston, TX, pp. 1002-1009, 1992.
- [2] E. Levi, "Multiphase electric machines for variable-speed applications," *IEEE Transactions on Ind. Electronics*, vol. 55, no. 5, pp. 1893-1909, 2008.
- [3] E. Levi, R. Bojoi, F. Profumo, H. A. Toliyat, and S. Williamson, "Multiphase induction motor drives - A technology status review," *IET Electric Power Applications*, vol. 1, no. 4, pp. 489-516, 2007.
- [4] S. Gataric, "A polyphase cartesian vector approach to control of polyphase AC machines," in *Proc. IEEE Industry Applications Society Annual Meeting IAS*, Rome, Italy, pp. 1648-1654, 2000.
- [5] S. Kouro, M. Malinowski, K. Gopakumar, G. Franquelo, J. Pou, J. Rodriguez, B. Wu, and A. Perez, "Recent advances and industrial applications of multilevel converters," *IEEE Transactions on Industrial Electronics*, vol. 57, no. 8, pp. 2553-2580, 2010.
- [6] J. Rodriguez, S. Bernet, B. Wu, J. O. Pontt, and S. Kouro, "Multilevel voltage-source-converter topologies for industrial medium-voltage drives," *IEEE Transactions on Industrial Electronics*, vol. 54, no. 6, pp. 2930-2945, 2007.
- [7] K. A. Corzine, S. D. Sudhoff, and C. A. Whitcomb, "Performance characteristics of a cascaded two-level converter," *IEEE Transactions on Energy Conversion*, vol. 14, no. 3, pp. 433-439, 1999.
- [8] B. A. Welchko and J. M. Nagashima, "A comparative evaluation of motor drive topologies for low-voltage, high-power EV/HEV propulsion systems," in *Proc. IEEE Int. Symp. on Ind. Elec. ISIE*, Rio de Janeiro, Brazil, pp. 379-384, 2003.
- [9] C. Rossi, G. Grandi, P. Corbelli, and D. Casadei, "Generation system for series hybrid powertrain based on dual two-level inverter," in *Proc. Eur.*

- Power Elec. and Appl. Conf. EPE*, Barcelona, Spain, CD-ROM paper 0978, 2009.
- [10] G. Grandi, C. Rossi, A. Lega, and D. Casadei, "Multilevel operation of a dual two-level inverter with power balancing capability," in *Proc. IEEE Industry Applications Society Annual Meeting IAS*, Tampa, FL, pp. 603-610, 2006.
- [11] Y. Kawabata, M. Nasu, T. Nomoto, E. C. Ejiogu and T. Kawabata, "High-efficiency and low acoustic noise drive system using open-winding AC motor and two space-vector-modulated inverters," *IEEE Transactions on Industrial Electronics*, vol. 49, no. 4, pp. 783-789, 2002.
- [12] N. Celanovic and D. Boroyevich, "A fast space-vector modulation algorithm for multilevel three-phase converters," *IEEE Transactions on Industry Applications*, vol. 37, no. 2, pp. 637-641, 2001.
- [13] C. M. Hutson, G. K. Venayagamoorthy, and K. A. Corzine, "Optimal SVM switching for a multilevel multi-phase machine using modified discrete PSO," in *Proc. IEEE Swarm Intelligence Symposium*, St. Louis, MO, CD-ROM, 2008.
- [14] Q. Song, X. Zhang, F. Yu, and C. Zhang, "Research on PWM techniques of five-phase three-level inverter," in *Proc. Int. Symp. on Power Elec., Electrical Drives, Automation and Motion SPEEDAM*, Taormina, Italy, pp. 561-565, 2006.
- [15] L. Gao and J. Fletcher, "A space vector switching strategy for three-level five-phase inverter drives," *IEEE Transactions on Industrial Electronics*, vol. 57, no. 7, pp. 2332-2343, 2010.
- [16] O. Dordevic, M. Jones, and E. Levi, "A space-vector PWM algorithm for a three-level seven-phase voltage source inverter," in *Proc. Eur. Power Elec. and Appl. Conf. EPE*, Birmingham, UK, CD-ROM paper 0123, 2011.
- [17] O. Lopez, J. Alvarez, J. Doval-Gandoy, and F. D. Freijeiro, "Multilevel multiphase space vector PWM algorithm with switching state redundancy," *IEEE Transactions on Industrial Electronics*, vol. 56, no. 3, pp. 792-804, 2009.
- [18] J. I. Leon, S. Vaquez, J. A. Sanchez, R. Portillo, L. G. Franquelo, J. M. Carrasco, and E. Dominguez, "Conventional space-vector modulation techniques versus the single-phase modulator for multilevel converters," *IEEE Transactions on Industrial Electronics*, vol. 57, no. 7, pp. 2473-2482, 2010.
- [19] K. K. Mohapatra and K. Gopakumar, "A novel split phase induction motor drive without harmonic filters and with linear voltage control for the full modulation range," *EPE Journal*, vol. 16, no. 4, pp. 20-28, 2006.
- [20] G. Grandi, A. Tani, P. Sanjeevikumar, and D. Ostojsic, "Multi-phase multi-level AC motor drive based on four three-phase two-level inverters," in *Proc. Int. Symp. on Power Elec., Electrical Drives, Automation and Motion SPEEDAM*, Pisa, Italy, pp. 1768-1775, 2010.
- [21] M. Jones, W. Satiawan, and E. Levi, "A five-phase multilevel space-vector PWM algorithm for a dual-inverter supplied drive," in *Proc. IEEE Industrial Electronics Society Annual Meeting IECON*, Glendale, AZ, pp. 2461-2466, 2010.
- [22] M. Jones, W. Satiawan, and E. Levi, "A three-level five-phase space-vector modulation algorithm based on the decomposition principle," in *Proc. IEEE Int. Elec. Machines and Drives Conf. IEMDC*, Niagara Falls, Canada, pp. 1235-1240, 2011.
- [23] N. Bodo, E. Levi, and M. Jones, "Carrier based modulation techniques for five-phase open-end winding topology," in *Proc. IEEE Industrial Electronics Society Annual Meeting IECON*, Melbourne, Australia, 2011.
- [24] N. Bodo, M. Jones, and E. Levi, "A PWM method for seven and nine phase open-end winding drives," in *Proc. Int. Conf. on Modelling and Simulation of Elec. Mach., Converters and Systems ELECTRMacs*, Paris, France, CD-ROM paper 0038, 2011.
- [25] D. Dujic, M. Jones, and E. Levi, "Generalized space vector PWM for sinusoidal output voltage generation with multiphase voltage source inverters," *Int. J. Ind. Elec. and Drives*, vol. 1, no. 1, pp. 1-13, 2009.
- [26] J. Rodriguez, L. G. Franquelo, S. Kouro, J. I. Leon, R. C. Portillo, M. A. M. Prats, and M. A. Perez, "Multilevel converters: An enabling technology for high-power applications," *Proceedings of the IEEE*, vol. 97, no. 11, pp. 1786-1817, 2009.
- [27] R. H. Wilkinson, T. A. Meynard, and H. du Toit Mouton, "Natural balance of multicell converters: The general case," *IEEE Transactions on Power Electronics*, vol. 21, no. 6, pp. 1658-1666, 2006.
- [28] G. Carrara, S. Gardella, M. Marchesoni, R. Salutari, and G. Sciutto, "A new multilevel PWM method: A theoretical analysis," *IEEE Transactions on Power Electronics*, vol. 7, no. 3, pp. 497-505, 1992.
- [29] E. C. de Santos and M. Pacas, "Fault-tolerant open-end winding motor drive systems," in *Proc. IEEE Industrial Electronics Society Annual Meeting IECON*, Melbourne, Australia, 2011.
- [30] D. Dujic, G. Grandi, M. Jones, and E. Levi, "A space vector PWM scheme for multi-frequency output voltage generation with multiphase voltage-source inverters," *IEEE Transactions on Industrial Electronics*, vol. 55, pp. 1943-1955, 2008.

APPENDIX

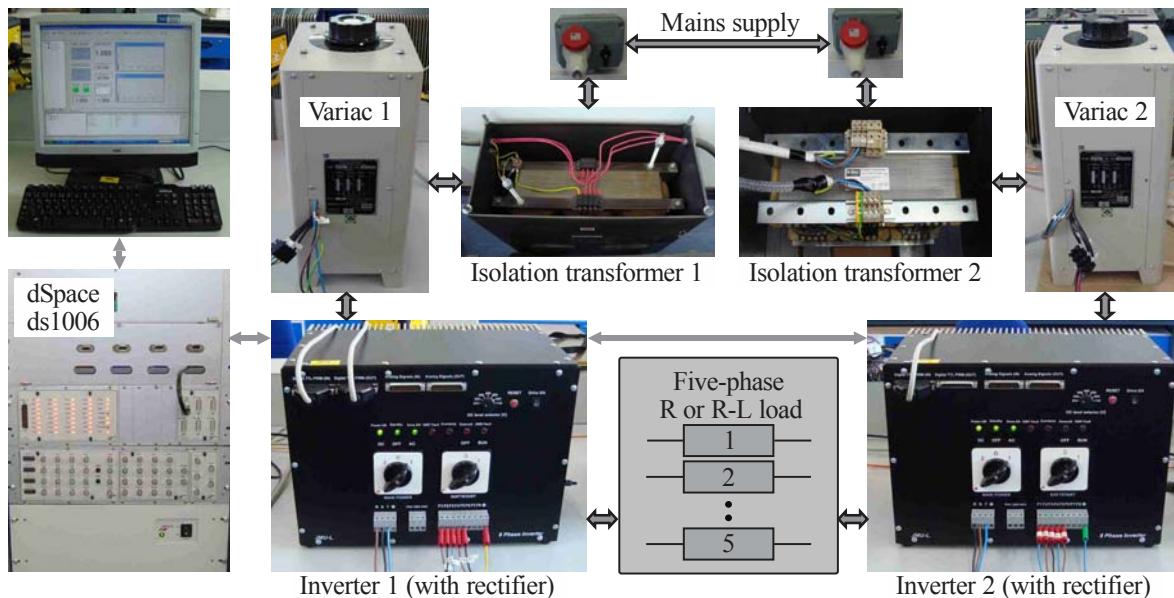


Fig. A1. Experimental set-up for the open-end winding configuration.